

# Task-Oriented Diffusion Model Compression

Geonung Kim, Beomsu Kim, Eunhyeok Park, Sunghyun Cho  
POSTECH

{k2woong92, qjatan0120, eh.park, s.cho}@postech.ac.kr

## Abstract

*As recent advancements in large-scale Text-to-Image (T2I) diffusion models have yielded remarkable high-quality image generation, diverse downstream Image-to-Image (I2I) applications have emerged. Despite the impressive results achieved by these I2I models, their practical utility is hampered by their large model size and the computational burden of the iterative denoising process. In this paper, we explore the compression potential of these I2I models in a task-oriented manner and introduce a novel method for reducing both model size and the number of timesteps. Through extensive experiments, we observe key insights and use our empirical knowledge to develop practical solutions that aim for near-optimal results with minimal exploration costs. We validate the effectiveness of our method by applying it to InstructPix2Pix for image editing and StableSR for image restoration. Our approach achieves satisfactory output quality with 39.2% and 56.4% reduction in model footprint and 81.4% and 68.7% decrease in latency to InstructPix2Pix and StableSR, respectively.*

## 1. Introduction

In the advent of large-scale text-to-image (T2I) diffusion models such as DALL-E [39], Stable Diffusion [42], and Imagen [45], there has been a dramatic improvement in image generation quality. This achievement has consequently opened up new opportunities across diverse applications, including image restoration [29, 55], image composition [14, 33, 47], image editing [5, 18, 40, 53, 56], conditional image synthesis [3, 15, 35, 61–64], panorama generation [4, 65], personalized generation [44], creature generation [41], and even 3D generation [8, 28, 37, 54].

While these applications employing T2I models have demonstrated unprecedented high-quality results, the extremely large parameter size combined with an iterative denoising process necessitates substantial computational resources, thus limiting their practicality. For instance, typical restoration networks generate images with fewer than 80 million parameters in a single feedforward pass [6, 7,

57, 59]. Meanwhile, StableSR [55], which utilizes Stable Diffusion [42] for image restoration tasks, requires approximately 916 million parameters with dozens of iterations. While StableSR provides a higher quality output, it requires at least 40 times additional latency, which is an unaffordable trade-off in many cases. Saving memory footprints and reducing the computation cost of diffusion models are key factors for their widespread adoption.

In response to this requirement, numerous studies have been actively conducted recently. These studies can be roughly categorized into two topics: reducing the number of denoising iterations [27, 30, 32, 34, 46, 49, 60] and reducing model footprint [25]. By focusing on the intrinsic features of diffusion models, these studies have proposed diverse task-agnostic optimization techniques. However, while they offer notable improvements for their respective directions, they have not yet produced results satisfactory in both metrics. To further reduce the implementation barrier of diffusion models, we must investigate the potential for more aggressive optimization opportunities.

Diffusion models are by default designed to generate high-quality output images from random noise. However, certain downstream applications involve input images that can provide more substantial guidance compared to noise. For example, in image editing tasks where high-quality images are already provided as input, the model needs to apply minor updates on top of the given informative inputs, which could greatly simplify the model’s structure and generation processes, but this task-oriented potential for compression remains unexplored.

In this work, we introduce a task-oriented diffusion model compression methodology, focusing on Image-to-Image (I2I) downstream tasks derived from large-scale T2I models. We hypothesize that due to the relative simplicity of our target I2I tasks compared to generative tasks, there are compression strategies uniquely suited to them that can provide significant benefits in both latency and memory footprint over existing task-agnostic techniques.

Our approach comprises two main components. Firstly, we introduce a depth-skip compression technique that effectively reduces model size and latency. Empirical experi-

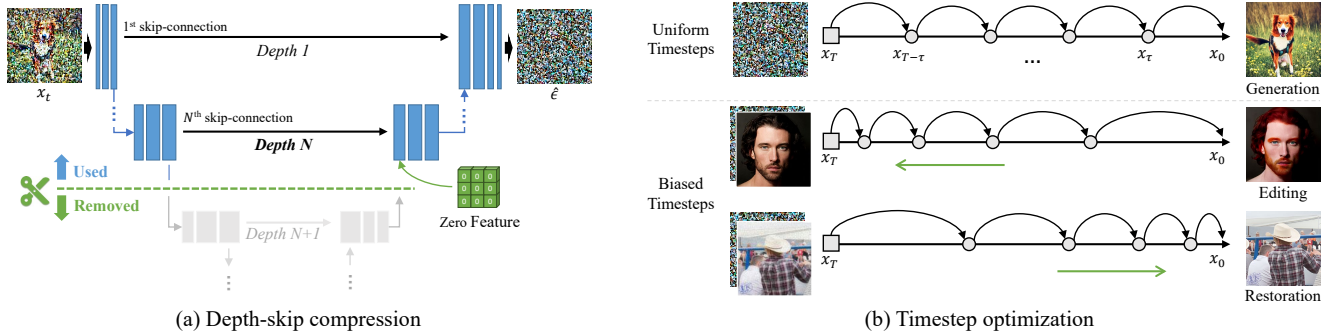


Figure 1. Overview of our methods. (a) Our depth-skip compression strategy eliminates all network blocks deeper than a specified skip-connection level, effectively reducing both the model size. (b) Our timestep optimization proposes an optimal sequence of timestep, given a fixed number of timesteps, based on biased timestep selection. Both approaches are highly effective in downstream Image-to-Image (I2I) that originates from a large-scale Text-to-Image (T2I) diffusion model.

ments confirm that the low-resolution encoded path, which primarily corresponds to coarse-grained features, are less impacted in various downstream tasks. By carefully pruning unnecessary paths and fine-tuning the model, we achieve performance benefits with negligible quality degradation. Secondly, we propose a timestep optimization method. We have observed that output quality significantly improves when focusing on a range of timestep that has a larger impact. Guided by this insight, we introduce an intuitive method that searches for the optimal sequence of timestep. Our combined method achieves satisfactory output quality with 60.8% parameter and 18.6% latency in Instruct-Pix2Pix [5] and 43.6% parameter and 31.3% latency in StableSR [55], respectively.

## 2. Related Works

### 2.1. I2I Downstream tasks from T2I

Since large-scale T2I models possess a rich generative prior for natural images, straightforward way for transferring T2I capabilities to downstream I2I tasks have achieved state-of-the-art performance in various domains, such as text-conditioned image inpainting [42], depth-conditioned generation [42], image restoration [29, 55], image editing [5], and conditional image synthesis [35, 64]. These methods utilize the entire parameters and the complete denoising process, despite the relative simplicity compared to the generative tasks that starts from Gaussian noise without any guidance images. In this paper, we explore the compression potential of these I2I models, taking into account both model footprint and denoising iterations.

### 2.2. Model Compression

The large footprint of diffusion models increases the need for model compression techniques to enhance their practical applicability. However, research in model compression has primarily focused on network architecture, in-

cluding compression techniques for Convolutional Neural Networks (CNNs) [16, 17, 26, 31] or Vision Transformer [9, 22, 36, 51, 52, 67]. Since these methods exclude the dynamics between the network and timestep, the potential for diffusion compression remains under-explored.

On a related note, BK-SDM [25] proposes a compression method for large-scale T2I models using block-removal knowledge distillation. While their method, similar to our depth-skip compression, involves removing network components with less impact and subsequently retraining the pruned model, their criteria for selecting network blocks to be removed appears somewhat arbitrary. For instance, they discard residual and attention layers situated in the middle of the network blocks without any theoretical or empirical justification. In contrast, our depth-skip compression is designed with a focus on task-oriented way and offers a more principled approach to identifying which blocks to remove, based on quality constraints of the target task. Furthermore, while their method solely concentrates on model compression, our approach encompasses both model compression and timestep optimization, making it more effective than their general approach in task-specific scenarios.

### 2.3. Timestep of Diffusion Models

For fast sampling, alternative ODE or SDE samplers have been proposed [30, 32, 49], achieving a significant reduction in iterations from 1000 steps to fewer than a hundred. Further reduction in iterations to less than 10 has been achieved through knowledge distillation techniques [34, 46]. While these methods do offer feasible reductions in time steps, the computational burden is considerable and often accompanied by noticeable quality degradation.

On the other hand, several methods aim to identify the optimal sampling schedule within a fixed number of iterations, either through differential optimization [60] or via genetic algorithms [27]. Despite substantially improving output fidelity in limited iterations, these approaches are com-

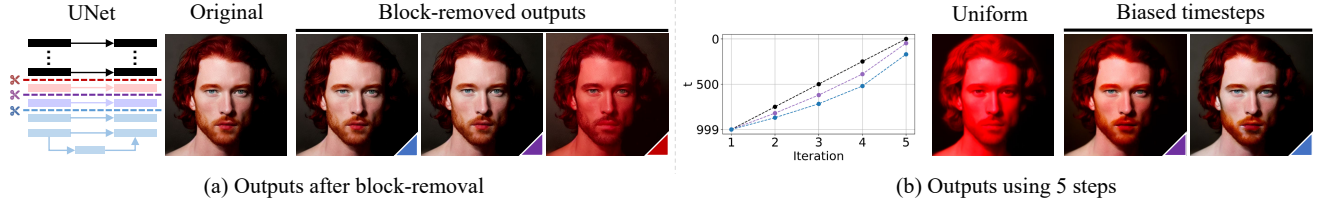


Figure 2. Observations applying block-removal and biased timestep to IP2P [5]. (a) Even after removing network-blocks beneath a certain skip connection, the output has little change. (b) by concentrating on earlier timestep, a viable output is obtained using 5 steps.

putationally expensive, requiring over a day to optimize even small-scale diffusion models for just 5 steps. This limitation adversely affects both the practicality and flexibility of these methods. In contrast, our proposed timestep optimization strategy requires less than an hour for optimization while delivering superior performance in task-specific scenarios.

### 3. Methods

In this section, we outline our methods. Specifically, we provide a brief explanation of the T2I diffusion model and transferred I2I model in Sec. 3.1. Next, we discuss the intuition and motivation behind our methods in Sec. 3.2. Subsequently, we introduce an approach called *depth-skip*, which is effective for reducing the number of parameters in Sec. 3.3. Finally, we describe our timestep optimization method, designed to find optimal timestep sequence given fixed iteration in Sec. 3.4.

#### 3.1. Diffusion Model

Diffusion models [21, 48, 50] are generative models that transform Gaussian noise into a target sample over a series of iterations, using a denoising process guided by a neural network. In the case of T2I diffusion models, a noise prediction network  $\epsilon_\theta$  is employed to estimate the noise component in the noised image  $x_t$  conditioned on timestep  $t$  and text prompt  $\mathcal{P}$ . For the downstream I2I tasks that leverage T2I models, the model is retrained using the loss formula as

$$\mathcal{L} = \|\epsilon_\theta(x_t, c_I, \mathcal{P}, t) - \epsilon\|^2, \quad (1)$$

where  $c_I$  represents an additional input image. To accommodate the additional input image, these approaches either fine-tune the diffusion model with minor modifications to the input network block [5, 42] or train a feature injection network while fixing the diffusion parameters [35, 55, 64].

#### 3.2. Motivation

For model compression, we assume that the deeper network layers of the UNet have a lesser impact on the output image in the transferred I2I model. This is because the coarse layers of generative models are primarily responsible for creating the image structure [23, 24], which is often unnecessary

for certain I2I tasks. Additionally, these coarser-level modules tend to have many channels, which consume a large amount of memory. By removing these channels, we can save footprint without compromising the output quality.

To validate this assertion, we conduct an experiment where we gradually remove the deepest network layers of IP2P [5] and check the output quality, as shown in Fig. 2 (a). Surprisingly, even after removing three sets of skip connections, the output quality remains comparable to the original. Please note that the outputs are achieved without additional fine-tuning after removing the skip connections; therefore, the coarse layers are scarcely utilized in IP2P tasks. We can observe a similar trend in different tasks. Inspired by this intuition, we introduce a depth-skip compression in Sec. 3.3, which effectively reduces the model parameter.

Regarding timestep optimization for transferred I2I models, we assume that the timestep with larger impact are biased towards one side. This assumption is based on existing research which suggests a division of roles between the early and latter timestep [2, 10, 11]. Specifically, earlier timestep is primarily involved in generation and the incorporation of prompt [2], while latter timestep is more concerned with image refinement [10, 11].

To validate this assertion, we conduct the IP2P task with only 5 steps at different intervals. In Fig. 2 (b), the black dashed line represents IP2P generation using uniform time sequence, while the purple and sky-blue dashed lines represent non-uniform with a focus on early timestep. As depicted in the figure, by prioritizing earlier timestep, we can attain viable results using only 5 steps. While there is variation in the preference for either earlier or later timestep, empirically similar phenomena were observed in other I2I tasks. This observation has inspired our approach to timestep optimization described in Sec. 3.4, where we aim to identify the optimal sequence of timestep given a fixed number of iterations.

Please note that in this study, we introduce two orthogonal methods, depth-skip compression and timestep optimization. Achieving optimal results by simultaneously applying both methods is highly challenging due to their enormous design space. In this paper, we present practical solutions based on extensive experiments. We have developed well-optimized solutions for both methods and observed

Baseline (Single depth)				(a) Fix param. & Min time ( $\Delta\text{PSNR} < 0.2 \text{ dB}$ )		(b) Fix time & Max quality ( $\Delta\text{Time} < 1\%$ )			(c) Fix quality & Min time ( $\Delta\text{PSNR} < 0.2 \text{ dB}$ )		
Depth	PSNR	Time(%)	Param(%)	Time(%)	$\Delta\text{Time}(\%)$	PSNR	$\Delta\text{PSNR}$	$\Delta\text{Param}(\%)$	Time(%)	$\Delta\text{Time}(\%)$	$\Delta\text{Param}(\%)$
11	32.86	89.91	79.17	86.44	-3.46	32.87	+0.02	+9.47	86.44	-3.46	+0.00
10	32.34	85.70	69.70	83.08	-2.62	32.68	+0.34	+9.47	81.11	-4.59	+9.47
9	31.39	82.78	60.77	78.51	-4.27	32.48	+1.08	+18.40	77.06	-5.72	+8.93
8	28.65	72.59	43.58	70.37	-2.23	30.18	+1.53	+26.13	66.30	-6.29	+26.13

Table 1. Comparisons between single and multi-depth searches applied to StableSR [55]. The percentages at “Time” and “Param”, which indicates parameter, are proportion to requirements in full model. The PSNR is measured based on outputs without depth-skip. This results suggest that our single depth approach efficiently searches the near-optimal point compared to a multi-depth search strategy.

---

#### Algorithm 1: Depth-search

---

**Input:** input image  $c_I$ , prompt  $\mathcal{P}$ , maximum depth  $d_{max}$ , metric function  $\mathcal{M}$

**Output:** Optimal depth  $d$

$d \leftarrow d_{max}$

$x_T \sim \mathcal{N}(0, I)$

**repeat**

$d \leftarrow d - 1$

$x \leftarrow \text{Sampler}_{DDIM}(x_T, c_I, \mathcal{P}; d)$

$m \leftarrow \mathcal{M}(x)$

**until** OverThreshold( $m$ );

---

that sequentially applying these methods consistently yields significantly favorable results. In the following sections, we will provide detailed explanations of each method.

### 3.3. Depth-Skip Compression

In this section, we describe the details of the depth-skip compression utilized for reducing model size and lowering inference latency. This method is implemented in the UNet [43] architecture, which is characterized by skip-connections that transfer features directly from the encoder to corresponding decoder blocks. The key concept is to ‘skip’ certain network blocks located beyond a predetermined ‘depth’ of the skip-connection. For example, a depth 8 model, denoted as  $D8$ , indicates skipping the network components situated beyond the 8th skip-connection, as shown in Fig. 1 (a). Our depth-skip compression consists of two steps: depth-search and fine-tuning. Firstly, we employ a depth-search technique to identify the target depth level. Specifically, using a predefined metric and threshold, we perform depth-skip starting from the deepest depth level and incrementally proceeding until meeting the quality threshold, as described in Alg. 1. After searching for the proper depth, we fine-tune the pruned model to further optimize its output quality.

#### 3.3.1 Discussions on multi-depth search

In our method, the search space is limited by globally selecting the skip level across all time steps. Although we have

designed our method in this manner to minimize search overhead, choosing the skip level for each time step could potentially yield additional performance benefits closer to the global optimum. In this section, we demonstrate that this alternative method offers marginal gains despite its exponentially growing search space.

First, we apply our technique, which skips a specific depth level globally, to the StableSR [55] task and measure the benefits of ours. Afterward, we employ brute-force search to identify solutions close to optimal for three different objectives for extensive analysis: achieving the fastest performance within restricted parameters, maximizing quality within a latency margin, and obtaining the fastest performance within a quality threshold. To manage search overhead, we limit the depth skip candidates from 7 to 12, use 10 denoising iterations, and assume that skip target can vary every two time steps. The overall results are summarized in Tab. 1, and the corresponding analysis on IP2P [5] is provided in Supplementary Material.

**Fix model size** When the model size is constrained, the pruned depth is uniformly applied across all time steps, same as our method. This is because, to maximize output quality, it is necessary to use all network blocks up to the allowed depth level for all time steps. Regarding latency, the improvement over our approach, while maintaining comparable quality, is at most 4.27% , as shown in Tab. 1 (a).

**Fix latency** When latency is constrained, different parts of the models are selectively used at various time steps. Because we need to retain all the parameters, there is no reduction in memory footprint. In terms of quality, although there are solutions that offer improved quality, the additional parameters required are substantial, as indicated in Tab. 1 (b). For instance, improving by 1.08 dB through greedy search necessitates an 18% increase in model size compared to ours at depth level 9.

**Fix quality** When some degree of quality degradation is acceptable, it is often possible to save on model size and latency. For instance, in StableSR, the outputs from depth levels 11 and 12 show comparable quality, allowing for the removal of redundant blocks at these levels. In terms of latency, while greedy search can identify faster solutions, the



---

**Algorithm 2: Timestep optimization**

---

**Input:** step size  $\eta$ , metric function  $\mathcal{M}$ , signum function  $\text{sgn}$ , small value  $\epsilon$ , GT iteration  $N$ , target iteration  $n$ ,

**Output:** Optimal timestep  $F_t(p_{prev}^s, n)$

$p \leftarrow 1, m \leftarrow \infty, x_T \sim \mathcal{N}(0, I)$

$x_{uni} \leftarrow \text{Sampler}_{DDIM}(x_T, c_I, \mathcal{P}, F_t(p, n))$

$x_{pos} \leftarrow \text{Sampler}_{DDIM}(x_T, c_I, \mathcal{P}, F_t(p + \epsilon, n))$

$x_{neg} \leftarrow \text{Sampler}_{DDIM}(x_T, c_I, \mathcal{P}, F_t((p + \epsilon)^{-1}, n))$

$s \leftarrow \text{sgn}(\mathcal{M}(x_{uni}, x_{neg}) - \mathcal{M}(x_{uni}, x_{pos}))$

$x^* \leftarrow \text{Sampler}_{DDIM}(x_T, c_I, \mathcal{P}, F_t(p, N))$

**repeat**

$m_{prev} \leftarrow m, p_{prev} \leftarrow p$

$p \leftarrow p + \eta$

$x \leftarrow \text{Sampler}_{DDIM}(x_T, c_I, \mathcal{P}, F_t(p^s, n))$

$m \leftarrow \mathcal{M}(x^*, x)$

**until**  $m > m_{prev}$ ;

---

trade-off with model size is also significant, as shown in Tab. 1 (c).

Overall, our simplified algorithm identifies close-to-optimal solutions with significantly smaller search overhead, while still maintaining our initial goal of reducing memory footprint and latency.

### 3.4. Timestep Optimization

In this section, we describe the details of our timestep optimization method, which aims to determine the optimal generation time sequence given a fixed number of iterations. Based on the intuition presented in Sec. 3.2 and Fig. 2 (b), we simplify the design space by searching for the slope of a gamma curve as follows:

$$F_t(\gamma, n) = T \cdot t^\gamma, \quad \gamma > 0$$
$$t = 0, \frac{1}{n-1}, \frac{2}{n-1}, \dots, 1 \quad (2)$$

Here,  $T$  represents the last timestep,  $\gamma$  is a parameter of the gamma curve, and  $n$  is the number of iterations. If  $\gamma > 1$ , the generation process concentrates on the early timestep of generation, while if  $0 < \gamma < 1$ , it focuses on the later timestep. Then, our optimization problem become to find a  $\gamma$  that produces the closest outputs to the original sampling results using a small  $n$ .

However, this straightforward optimization often leads to unsatisfactory results due to the fixed nature of the first and last timestep. To alleviate this limitation, we apply a scale-down mechanism for the gamma curve. Specifically, we scale down the gamma curve toward  $T$  when  $\gamma < 1$  proportional to decrease of  $\gamma$  value, and vice versa. The formal definition is as follows:

$$F_t(\gamma, n) = T \cdot t^\gamma, \quad \gamma > 0 \quad (3)$$

$$t' = \frac{t - t_l}{t_u - t_l}, \quad t = 0, \frac{T}{n-1}, \frac{2T}{n-1}, \dots, T \quad (4)$$

$$(t_l, t_u) = \begin{cases} (0, T + \alpha(\gamma - 1)), & \gamma \geq 1 \\ (\alpha(1 - 1/\gamma), T), & \gamma < 1 \end{cases} \quad (5)$$

where  $\alpha$  is a coefficient for scale strength. This adjustment allows for greater flexibility and potentially more effective optimization of the timestep.

The search process consists of two stages. Firstly, we determine whether  $\gamma$  increases or decreases by evaluating which direction yields better outputs. Following this, we perform a greedy search by progressively increasing or decreasing the value of  $\gamma$  until there is no further improvement in quality, as described in Alg. 2.

## 4. Experiments

In this section, we offer a comprehensive assessment of the efficiency and efficacy of our method. Sec. 4.1 demonstrates the qualitative results obtained through the application of our method. Sec. 4.2 and Sec. 4.3 provide detailed analyses of depth-skip compression and timestep optimization, respectively. Sec. 4.4 compares our method with a previous state-of-the-art approach, AutoDiffusion [27]. Sec. 4.5 showcases various applications where our method is employed in different downstream tasks. It is important to note that when discussing computational resources, including memory footprint and latency, our focus is exclusively on the diffusion UNet. This excludes considerations for the text-encoder [38] and the auto-encoder [12].

**Implementation details** We conducted evaluations of our methods on two tasks: image editing with IP2P [5] and image restoration with StableSR [55]. For the depth-skip compression, we set the PSNR threshold at 28 dB, using the ground truth based on 50 iteration results for StableSR [55]. Regarding IP2P [5], we utilized a combination of CLIP image similarity [38] and directional CLIP similarity [13], which are the same metrics employed by IP2P to measure performance. The threshold values for these metrics were set at 0.7 and 0.2, respectively. For fine-tuning, we utilized the same dataset and training strategy as the original method. In the case of timestep optimization, we employed a bias coefficient of  $\alpha = 30$  and the PSNR metric, utilizing 50-step results from DDIM [49] deterministic process. Both for depth-skip and timestep optimization, we employed 100 samples for optimization process.

### 4.1. Qualitative Results

Fig. 3 illustrates the generated results after applying depth-skip compression and timestep optimization. The label “Original” represents outputs obtained by the full model

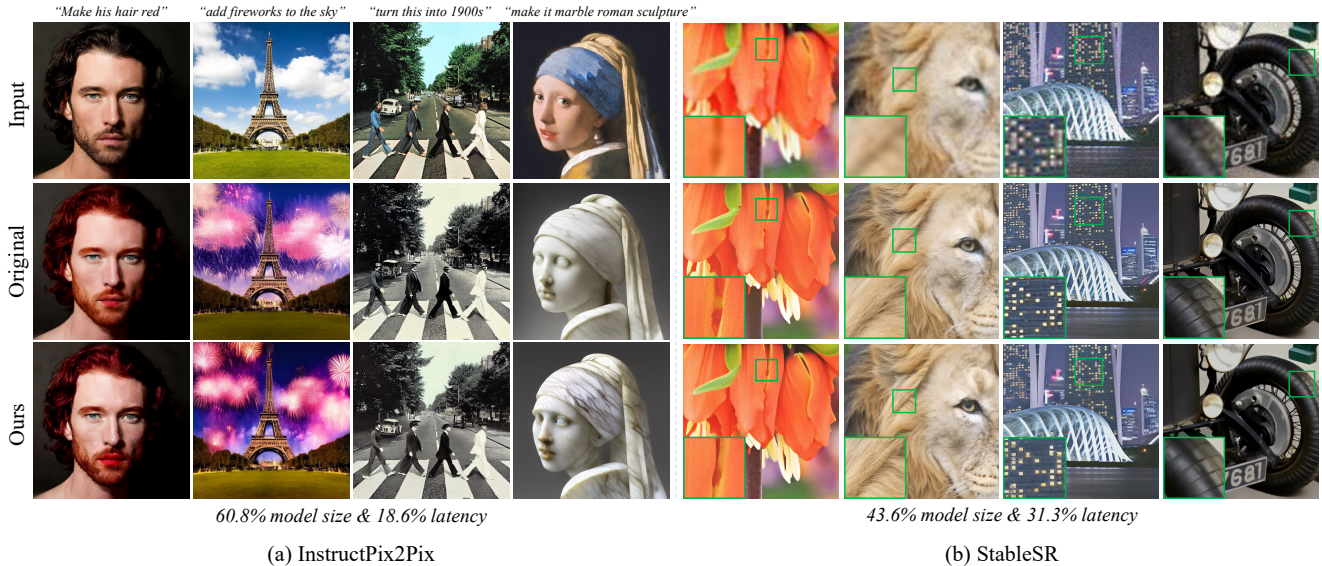


Figure 3. We achieve satisfactory output images with significantly reduced model size and latency, as described on top of the caption, after applying our method to InstructPix2Pix [5] and StableSR [55].

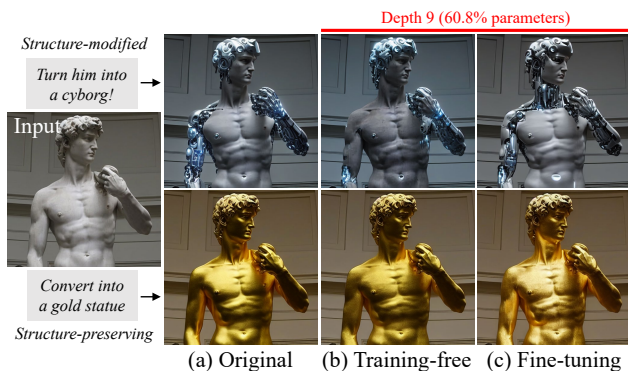


Figure 4. Qualitative comparison of depth-skip compression in training-free and fine-tuning applied to IP2P [5]. Ours significantly reduces model size while preserving editing performance.

with 50-step, which is a commonly used number of iterations in practice. Our IP2P [5] and StableSR [55] results are achieved using reduced parameters and iterations:  $D9$  with 60.8% of the parameters and 10 steps for IP2P, and  $D8$  with 43.6% of the parameters and 20 steps for StableSR. As a result of the reductions in iterations and parameters, the latencies of IP2P and StableSR have been reduced to 18.6% and 31.3%, respectively.

## 4.2. Depth-skip Compression

In this section, we conduct ablation studies using our depth-skip compression only.

**InstructPix2Pix** The selected depth is  $D9$  using 60.8% model parameters. Fig. 4 shows the qualitative comparison between training-free and fine-tuning using  $D9$  model. For

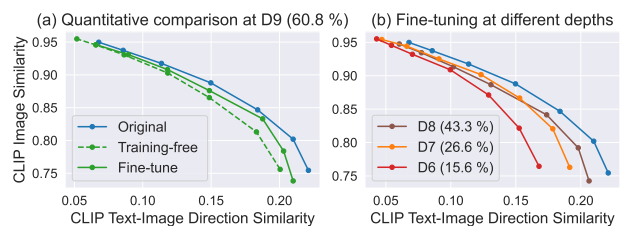


Figure 5. Trade-off between consistency of input image and editing for various depth-skip configurations applied to IP2P [5].

structure-modified editing, the training-free outcomes show weakened editing strength, as seen in the first row, but the editing quality is notably recovered after fine-tuning. Regarding structure-preserved editing, the training-free results show comparable quality to the original outcomes.

For quantitative comparison, we plot trade-off values of CLIP image similarity [38] and directional CLIP similarity [13]. These values indicate input image and editing prompt consistencies, which is the same evaluation framework used in IP2P [5]. Each dots in the plot corresponds to various image CFG [20] values ranging of [1.0, 2.2].

As shown in Fig. 5 (a), fine-tuning has the benefit of recovering the quality degradation of model pruning. Furthermore, we extend our depth-skip to lower depth levels, as shown in Fig. 5 (b). Although the quality gradually deteriorates as depth level decreases, some editing operations still work even at  $D6$ . For more detailed discussions, please refer to the Supplementary Material.

**StableSR** The depth is picked as  $D8$  in StableSR, which uses 43.6% parameters. As shown in Fig. 6 (d), our pruned



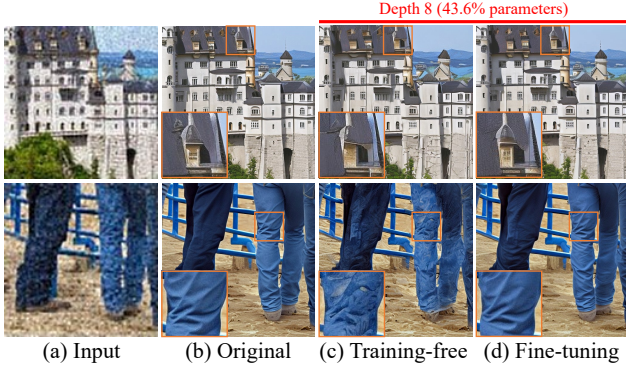


Figure 6. Qualitative comparison of depth-skip compression in training-free and fine-tuning scenarios applied to StableSR [55].

Model	FID↓	PSNR↑	LPIPS↓	Parameter
Original	27.70	21.51	0.437	917M (100%)
<i>D8</i> (Training-free)	40.25	21.40	0.467	400M (43.6%)
<i>D8</i> (Fine-tune)	30.15	21.48	0.449	400M (43.6%)

Table 2. Quantitative comparison of depth-skip to StableSR [55]. After fine-tuning, FID is significantly restored.

	InstructPix2Pix		StableSR	
	Time(s)	MACs(T)	Time(s)	MACs(T)
Original	6.312	50.81	2.807	18.75
<i>D9</i>	5.978	47.27	2.421	17.49
<i>D8</i>	5.685	41.75	2.204	15.57

Table 3. Latency and MACs [66] improvement after depth-skip. 50 iterations and RTX3090 GPU are used.

model produces qualitatively comparable results to the original. Quantitative comparison is conducted using the synthetic DIV2K [1] validation set, which is also employed for testing in StableSR [55]. As shown in Tab. 2, the FID [19] metric is improved by 10.1 after fine-tuning, with a difference of less than 3 compared to the original.

**Latency and Computation** Due to our depth-skip compression, which significantly reduces the model size, both latency and computational load have also improved, as presented in Tab. 3. To be specific, we have achieved reductions of 5.3% and 6.97% in latency and computation for IP2P, and 21.5% and 17.0% in latency and computation for StableSR, respectively.

### 4.3. Timestep Optimization

In this section, we conduct ablation studies using our timestep optimization only. Fig. 7 shows the results of IP2P [5] using different iterations with uniform and optimized timestep. Our optimized approach achieves outcomes closer to the original, especially with fewer iterations. Regarding StableSR [55], Tab. 8 shows that optimized timestep produce better edge and texture elements within

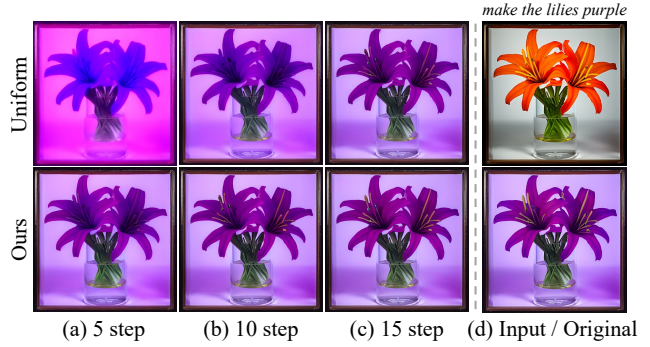


Figure 7. Ours achieves outcomes closer to original than uniform timestep in IP2P [5].



Figure 8. Qualitative comparison of timestep optimization to StableSR [55] using 20 steps. Ours produces better texture and edge elements than uniform time sequence.

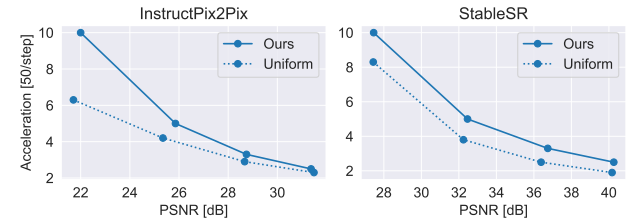


Figure 9. We plot speeds to reach comparable PSNR with original sample for uniform timestep and ours. For all cases, we achieve same PSNR faster than uniform timestep.

the same iterations. Fig. 9 presents a plot of the speeds required to achieve comparable PSNR with the original sample for both uniform and optimized timestep. Our method outperforms the uniform timestep strategy across various levels of accuracy. Specifically, our optimal timestep for IP2P using 5 steps is 1.6 times faster than the uniform approach. Additionally, the figure suggests that given the high-level PSNR achieved with a relatively small iteration in a uniform way, the conventional practice of using 50 iterations is unnecessarily excessive for these I2I tasks. We also observed that the optimized timestep have little change after applying depth-skip compression. On the other hand, it varies in changes of CFG [20] values. For related analysis and additional quantitative comparisons, please refer to the Supplementary Material.

	Step	Ours	AutoDiffusion			
		T	T	T+L	$\Delta$ PSNR	$\Delta$ Time
IP2P	5	<b>22.00</b>	20.64	20.64	0.00	-0.0%
	10	<b>25.86</b>	24.79	24.61	-0.18	-0.2%
StableSR	5	<b>27.46</b>	26.58	26.23	-0.35	-2.7%
	10	<b>32.46</b>	29.03	27.80	-1.23	-2.8%

Table 4. Quantitative comparison with AutoDiffusion [27]. “T” and “T+L” indicate the PSNR metrics for the timestep optimization and additional network skipping, respectively. “ $\Delta$ PSNR” and “ $\Delta$ Time” represent degradation and latency reduction after layer-skip, respectively. Ours outperforms in timestep optimization, while the benefits gained from layer-skip are marginal.

	IP2P		StableSR	
	5 step	10 step	5 step	10 step
AutoDiffusion [27]	40.5 h	75.1 h	16.3 h	27.1 h
Ours	<b>38.7 m</b>	<b>30.9 m</b>	<b>9.5 m</b>	<b>11.1 m</b>

Table 5. The time required for timestep optimization. Our method is significantly faster than AutoDiffusion [27].

#### 4.4. Comparison with AutoDiffusion

In this section, we compare our method with a state-of-the-art technique, AutoDiffusion [27], which jointly optimizes the timestep and skip configuration of network layers using an evolutionary search. For optimization, we employ the same criterion and the number of samples as in our timestep optimization. Tab. 4 illustrates that our method outperforms AutoDiffusion [27] in timestep optimization. Regarding the layer-skip search, the acceleration achieved is marginal, and there is a noticeable performance trade-off. Furthermore, AutoDiffusion’s layer-skip search fails to find skip configurations that remove network parameters, as demonstrated in Fig. 10. In terms of the time required for optimization, our method takes less than an hour, whereas AutoDiffusion [27] generally requires more than a day, as indicated in Tab. 5. Since optimal timestep depends on CFG [20] values, as described in Sec. 4.3, their expensive search cost significantly hampers the practical usage. For more detailed comparisons, please refer to the Supplementary Material.

#### 4.5. Applications

To show a versatility of our method, we apply our method to high-frequency synthesis and image inpainting tasks.

**High-frequency synthesis** A recent approach to image restoration involves combining a regression approach, which is weak in handling high-frequency details, with a generative prior method, which may lack content consistency [58]. In this application, our method serves as the generative prior component. For transfer learning, we utilize Stable Diffusion [42] as upstream model. Fig. 11 (a) demonstrates that our model successfully generates high-

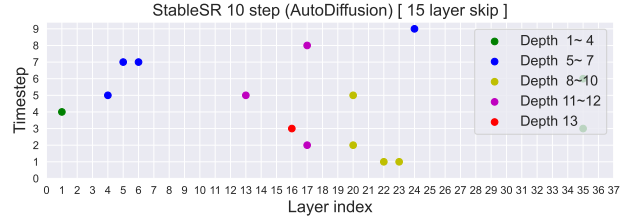
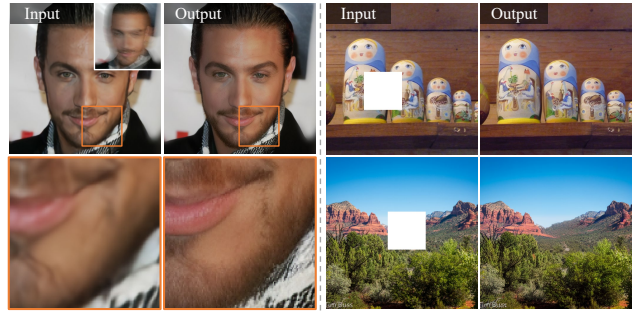


Figure 10. Layer-skip results of AutoDiffusion. The colored dots indicate the layers that are skipped at each timestep. A layer to be removed must be selected across all timestep. They fail to identify layers to be discarded.



(a) High-frequency Synthesis (b) Image Inpainting

Figure 11. We apply our method to other downstream tasks: high-frequency synthesis and inpainting.

frequency details over images restored by HINet [6], using only 26.6% of the parameters and 20 steps.

**Image inpainting** We adapt a text-conditioned image inpainting model [42] for unconditional inpainting tasks. Fig. 11 (b) illustrates that our model can generate plausible content, utilizing 43.3% of the parameters and 15 steps.

## 5. Conclusions

In this paper, we introduce a novel task-oriented compression method that combines depth-skip compression, reducing model size by pruning coarse network layers, and timestep optimization, finding the optimal timestep sequence using a scaled-gamma curve. We validate our method with IP2P [5] and StableSR [55], achieving practical results, including a 39.2% reduction in parameters and an 81.4% reduction in latency for IP2P, and a 56.4% reduction in parameters and a 68.7% reduction in latency for StableSR.

**Limitation & Future work** While timestep optimization demonstrates effectiveness in small iterations, it faces challenges in achieving comparable performance with significantly reduced iterations, which is a fundamental limitation of optimizing the time schedule [27, 60]. Therefore, our future work will focus on achieving comparable quality with significantly fewer iterations by applying a distillation method [34, 46] in a task-oriented manner.



## References

- [1] Eirikur Agustsson and Radu Timofte. Ntire 2017 challenge on single image super-resolution: Dataset and study. In *The IEEE Conference on Computer Vision and Pattern Recognition (CVPR) Workshops*, 2017. 7
- [2] Yogesh Balaji, Seungjun Nah, Xun Huang, Arash Vahdat, Jiaming Song, Karsten Kreis, Miika Aittala, Timo Aila, Samuli Laine, Bryan Catanzaro, et al. ediffi: Text-to-image diffusion models with an ensemble of expert denoisers. *arXiv preprint arXiv:2211.01324*, 2022. 3
- [3] Arpit Bansal, Hong-Min Chu, Avi Schwarzschild, Soumyadip Sengupta, Micah Goldblum, Jonas Geiping, and Tom Goldstein. Universal guidance for diffusion models. In *CVPR*, pages 843–852, 2023. 1
- [4] Omer Bar-Tal, Lior Yariv, Yaron Lipman, and Tali Dekel. Multidiffusion: Fusing diffusion paths for controlled image generation. *International Conference on Machine Learning*, 2023. 1
- [5] Tim Brooks, Aleksander Holynski, and Alexei A Efros. Instructpix2pix: Learning to follow image editing instructions. In *CVPR*, pages 18392–18402, 2023. 1, 2, 3, 4, 5, 6, 7, 8
- [6] Liangyu Chen, Xin Lu, Jie Zhang, Xiaojie Chu, and Chengpeng Chen. Hinet: Half instance normalization network for image restoration. In *Proceedings of the IEEE/CVF Conference on Computer Vision and Pattern Recognition*, pages 182–192, 2021. 1, 8
- [7] Liangyu Chen, Xiaojie Chu, Xiangyu Zhang, and Jian Sun. Simple baselines for image restoration. In *European Conference on Computer Vision*, pages 17–33. Springer, 2022. 1
- [8] Rui Chen, Yongwei Chen, Ningxin Jiao, and Kui Jia. Fantasia3d: Disentangling geometry and appearance for high-quality text-to-3d content creation. *ICCV*, 2023. 1
- [9] Tianlong Chen, Yu Cheng, Zhe Gan, Lu Yuan, Lei Zhang, and Zhangyang Wang. Chasing sparsity in vision transformers: An end-to-end exploration. *Advances in Neural Information Processing Systems*, 34:19974–19988, 2021. 2
- [10] Jooyoung Choi, Jungbeom Lee, Chaehun Shin, Sungwon Kim, Hyunwoo Kim, and Sungroh Yoon. Perception prioritized training of diffusion models. In *CVPR*, pages 11472–11481, 2022. 3
- [11] Kamil Deja, Anna Kuzina, Tomasz Trzcinski, and Jakub Tomczak. On analyzing generative and denoising capabilities of diffusion-based deep generative models. *NeurIPS*, 35:26218–26229, 2022. 3
- [12] Patrick Esser, Robin Rombach, and Bjorn Ommer. Taming transformers for high-resolution image synthesis. In *Proceedings of the IEEE/CVF conference on computer vision and pattern recognition*, pages 12873–12883, 2021. 5
- [13] Rinon Gal, Or Patashnik, Haggai Maron, Amit H Bermano, Gal Chechik, and Daniel Cohen-Or. Stylegan-nada: Clip-guided domain adaptation of image generators. *ACM Transactions on Graphics (TOG)*, 41(4):1–13, 2022. 5, 6
- [14] Roy Hachnochi, Mingrui Zhao, Nadav Orzech, Rinon Gal, Ali Mahdavi-Amiri, Daniel Cohen-Or, and Amit Haim Bermano. Cross-domain compositing with pretrained diffusion models. *arXiv preprint arXiv:2302.10167*, 2023. 1
- [15] Cusuh Ham, James Hays, Jingwan Lu, Krishna Kumar Singh, Zhifei Zhang, and Tobias Hinz. Modulating pretrained diffusion models for multimodal image synthesis. *SIGGRAPH Conference Proceedings*, 2023. 1
- [16] Yihui He, Xiangyu Zhang, and Jian Sun. Channel pruning for accelerating very deep neural networks. In *Proceedings of the IEEE international conference on computer vision*, pages 1389–1397, 2017. 2
- [17] Yang He, Ping Liu, Ziwei Wang, Zhilan Hu, and Yi Yang. Filter pruning via geometric median for deep convolutional neural networks acceleration. In *Proceedings of the IEEE/CVF conference on computer vision and pattern recognition*, pages 4340–4349, 2019. 2
- [18] Amir Hertz, Kfir Aberman, and Daniel Cohen-Or. Delta denoising score. In *ICCV*, pages 2328–2337, 2023. 1
- [19] Martin Heusel, Hubert Ramsauer, Thomas Unterthiner, Bernhard Nessler, and Sepp Hochreiter. Gans trained by a two time-scale update rule converge to a local nash equilibrium. *Advances in neural information processing systems*, 30, 2017. 7
- [20] Jonathan Ho and Tim Salimans. Classifier-free diffusion guidance. *arXiv preprint arXiv:2207.12598*, 2022. 6, 7, 8
- [21] Jonathan Ho, Ajay Jain, and Pieter Abbeel. Denoising diffusion probabilistic models. pages 6840–6851, 2020. 3
- [22] Ding Jia, Kai Han, Yunhe Wang, Yehui Tang, Jianyuan Guo, Chao Zhang, and Dacheng Tao. Efficient vision transformers via fine-grained manifold distillation. *arXiv e-prints*, pages arXiv–2107, 2021. 2
- [23] Tero Karras, Samuli Laine, and Timo Aila. A style-based generator architecture for generative adversarial networks. In *CVPR*, pages 4401–4410, 2019. 3
- [24] Tero Karras, Samuli Laine, Miika Aittala, Janne Hellsten, Jaakko Lehtinen, and Timo Aila. Analyzing and improving the image quality of stylegan. In *CVPR*, pages 8110–8119, 2020. 3
- [25] Bo-Kyeong Kim, Hyoung-Kyu Song, Thibault Castells, and Shinkook Choi. Bk-sdm: Architecturally compressed stable diffusion for efficient text-to-image generation. *ICML Workshop on Efficient Systems for Foundation Models (ES-FoMo)*, 2023. 1, 2
- [26] Hao Li, Asim Kadav, Igor Durdanovic, Hanan Samet, and Hans Peter Graf. Pruning filters for efficient convnets. *arXiv preprint arXiv:1608.08710*, 2016. 2
- [27] Lijiang Li, Huixia Li, Xiawu Zheng, Jie Wu, Xuefeng Xiao, Rui Wang, Min Zheng, Xin Pan, Fei Chao, and Rongrong Ji. Autodiffusion: Training-free optimization of time steps and architectures for automated diffusion model acceleration. In *ICCV*, pages 7105–7114, 2023. 1, 2, 5, 8
- [28] Chen-Hsuan Lin, Jun Gao, Luming Tang, Towaki Takikawa, Xiaohui Zeng, Xun Huang, Karsten Kreis, Sanja Fidler, Ming-Yu Liu, and Tsung-Yi Lin. Magic3d: High-resolution text-to-3d content creation. In *CVPR*, pages 300–309, 2023. 1
- [29] Xinqi Lin, Jingwen He, Ziyang Chen, Zhaoyang Lyu, Ben Fei, Bo Dai, Wanli Ouyang, Yu Qiao, and Chao Dong. Diffbir: Towards blind image restoration with generative diffusion prior. *arXiv preprint arXiv:2308.15070*, 2023. 1, 2

- [30] Luping Liu, Yi Ren, Zhijie Lin, and Zhou Zhao. Pseudo numerical methods for diffusion models on manifolds. 2022. [1](#), [2](#)
- [31] Zhuang Liu, Jianguo Li, Zhiqiang Shen, Gao Huang, Shoumeng Yan, and Changshui Zhang. Learning efficient convolutional networks through network slimming. In *Proceedings of the IEEE international conference on computer vision*, pages 2736–2744, 2017. [2](#)
- [32] Cheng Lu, Yuhao Zhou, Fan Bao, Jianfei Chen, Chongxuan Li, and Jun Zhu. Dpm-solver: A fast ode solver for diffusion probabilistic model sampling in around 10 steps. *NeurIPS*, 35:5775–5787, 2022. [1](#), [2](#)
- [33] Shilin Lu, Yanzhu Liu, and Adams Wai-Kin Kong. Tf-icon: Diffusion-based training-free cross-domain image composition. In *ICCV*, pages 2294–2305, 2023. [1](#)
- [34] Chenlin Meng, Robin Rombach, Ruiqi Gao, Diederik Kingma, Stefano Ermon, Jonathan Ho, and Tim Salimans. On distillation of guided diffusion models. In *CVPR*, pages 14297–14306, 2023. [1](#), [2](#), [8](#)
- [35] Chong Mou, Xintao Wang, Liangbin Xie, Jian Zhang, Zhonggang Qi, Ying Shan, and Xiaohu Qie. T2i-adapter: Learning adapters to dig out more controllable ability for text-to-image diffusion models. *arXiv preprint arXiv:2302.08453*, 2023. [1](#), [2](#), [3](#)
- [36] Bowen Pan, Rameswar Panda, Rogerio Schmidt Feris, and Aude Jeanne Oliva. Interpretability-aware redundancy reduction for vision transformers, 2023. US Patent App. 17/559,053. [2](#)
- [37] Ben Poole, Ajay Jain, Jonathan T Barron, and Ben Mildenhall. Dreamfusion: Text-to-3d using 2d diffusion. *ICLR*, 2023. [1](#)
- [38] Alec Radford, Jong Wook Kim, Chris Hallacy, Aditya Ramesh, Gabriel Goh, Sandhini Agarwal, Girish Sastry, Amanda Askell, Pamela Mishkin, Jack Clark, et al. Learning transferable visual models from natural language supervision. In *International conference on machine learning*, pages 8748–8763. PMLR, 2021. [5](#), [6](#)
- [39] Aditya Ramesh, Mikhail Pavlov, Gabriel Goh, Scott Gray, Chelsea Voss, Alec Radford, Mark Chen, and Ilya Sutskever. Zero-shot text-to-image generation. In *International Conference on Machine Learning*, pages 8821–8831. PMLR, 2021. [1](#)
- [40] Hareesh Ravi, Sachin Kelkar, Midhun Harikumar, and Ajinkya Kale. Preditor: Text guided image editing with diffusion prior. *arXiv preprint arXiv:2302.07979*, 2023. [1](#)
- [41] Elad Richardson, Kfir Goldberg, Yuval Alaluf, and Daniel Cohen-Or. Conceptlab: Creative generation using diffusion prior constraints. *arXiv preprint arXiv:2308.02669*, 2023. [1](#)
- [42] Robin Rombach, Andreas Blattmann, Dominik Lorenz, Patrick Esser, and Björn Ommer. High-resolution image synthesis with latent diffusion models. In *CVPR*, pages 10684–10695, 2022. [1](#), [2](#), [3](#), [8](#)
- [43] Olaf Ronneberger, Philipp Fischer, and Thomas Brox. U-net: Convolutional networks for biomedical image segmentation. *CoRR*, abs/1505.04597, 2015. [4](#)
- [44] Nataniel Ruiz, Yuanzhen Li, Varun Jampani, Yael Pritch, Michael Rubinstein, and Kfir Aberman. Dreambooth: Fine tuning text-to-image diffusion models for subject-driven generation. In *CVPR*, pages 22500–22510, 2023. [1](#)
- [45] Chitwan Saharia, William Chan, Saurabh Saxena, Lala Li, Jay Whang, Emily L Denton, Kamyar Ghasemipour, Raphael Gontijo Lopes, Burcu Karagol Ayan, Tim Salimans, et al. Photorealistic text-to-image diffusion models with deep language understanding. *NeurIPS*, 35:36479–36494, 2022. [1](#)
- [46] Tim Salimans and Jonathan Ho. Progressive distillation for fast sampling of diffusion models. In *ICLR*, 2022. [1](#), [2](#), [8](#)
- [47] Vishnu Sarukkai, Linden Li, Arden Ma, Christopher Ré, and Kayvon Fatahalian. Collage diffusion. *arXiv preprint arXiv:2303.00262*, 2023. [1](#)
- [48] Jascha Sohl-Dickstein, Eric Weiss, Niru Maheswaranathan, and Surya Ganguli. Deep unsupervised learning using nonequilibrium thermodynamics. In *International conference on machine learning*, pages 2256–2265. PMLR, 2015. [3](#)
- [49] Jiaming Song, Chenlin Meng, and Stefano Ermon. Denoising diffusion implicit models. 2021. [1](#), [2](#), [5](#)
- [50] Yang Song, Jascha Sohl-Dickstein, Diederik P Kingma, Abhishek Kumar, Stefano Ermon, and Ben Poole. Score-based generative modeling through stochastic differential equations. *ICLR*, 2021. [3](#)
- [51] Yehui Tang, Kai Han, Yunhe Wang, Chang Xu, Jianyuan Guo, Chao Xu, and Dacheng Tao. Patch slimming for efficient vision transformers. In *Proceedings of the IEEE/CVF Conference on Computer Vision and Pattern Recognition*, pages 12165–12174, 2022. [2](#)
- [52] Hugo Touvron, Matthieu Cord, Matthijs Douze, Francisco Massa, Alexandre Sablayrolles, and Hervé Jégou. Training data-efficient image transformers & distillation through attention. In *International conference on machine learning*, pages 10347–10357. PMLR, 2021. [2](#)
- [53] Narek Tumanyan, Michal Geyer, Shai Bagon, and Tali Dekel. Plug-and-play diffusion features for text-driven image-to-image translation. In *CVPR*, pages 1921–1930, 2023. [1](#)
- [54] Haochen Wang, Xiaodan Du, Jiahao Li, Raymond A Yeh, and Greg Shakhnarovich. Score jacobian chaining: Lifting pretrained 2d diffusion models for 3d generation. In *CVPR*, pages 12619–12629, 2023. [1](#)
- [55] Jianyi Wang, Zongsheng Yue, Shangchen Zhou, Kelvin CK Chan, and Chen Change Loy. Exploiting diffusion prior for real-world image super-resolution. *arXiv preprint arXiv:2305.07015*, 2023. [1](#), [2](#), [3](#), [4](#), [5](#), [6](#), [7](#), [8](#)
- [56] Qian Wang, Biao Zhang, Michael Birsak, and Peter Wonka. Mdp: A generalized framework for text-guided image editing by manipulating the diffusion path. *arXiv preprint arXiv:2303.16765*, 2023. [1](#)
- [57] Xintao Wang, Yu Li, Honglun Zhang, and Ying Shan. Towards real-world blind face restoration with generative facial prior. In *Proceedings of the IEEE/CVF conference on computer vision and pattern recognition*, pages 9168–9178, 2021. [1](#)
- [58] Yujin Wang, Lingen Li, Tianfan Xue, and Jinwei Gu. Reconstruct-and-generate diffusion model for detail-preserving image denoising, 2023. [8](#)

- [59] Zhendong Wang, Xiaodong Cun, Jianmin Bao, Wengang Zhou, Jianzhuang Liu, and Houqiang Li. Uformer: A general u-shaped transformer for image restoration. In *Proceedings of the IEEE/CVF conference on computer vision and pattern recognition*, pages 17683–17693, 2022. 1
- [60] Daniel Watson, William Chan, Jonathan Ho, and Mohammad Norouzi. Learning fast samplers for diffusion models by differentiating through sample quality. In *ICLR*, 2021. 1, 2, 8
- [61] Jinheng Xie, Yuexiang Li, Yawen Huang, Haozhe Liu, Wentian Zhang, Yefeng Zheng, and Mike Zheng Shou. Boxdiff: Text-to-image synthesis with training-free box-constrained diffusion. In *ICCV*, pages 7452–7461, 2023. 1
- [62] Binbin Yang, Yi Luo, Ziliang Chen, Guangrun Wang, Xiaodan Liang, and Liang Lin. Law-diffusion: Complex scene generation by diffusion with layouts. In *Proceedings of the IEEE/CVF International Conference on Computer Vision*, pages 22669–22679, 2023.
- [63] Jiwen Yu, Yinhuai Wang, Chen Zhao, Bernard Ghanem, and Jian Zhang. Freedom: Training-free energy-guided conditional diffusion model. *ICCV*, 2023.
- [64] Lvmin Zhang, Anyi Rao, and Maneesh Agrawala. Adding conditional control to text-to-image diffusion models. In *CVPR*, pages 3836–3847, 2023. 1, 2, 3
- [65] Qinsheng Zhang, Jiaming Song, Xun Huang, Yongxin Chen, and Ming-Yu Liu. Diffcollage: Parallel generation of large content with diffusion models. *CVPR*, 2023. 1
- [66] L. Zhu. Thop. <https://github.com/Lyken17/pytorch-OpCounter>, 2019. 7
- [67] Mingjian Zhu, Yehui Tang, and Kai Han. Vision transformer pruning. *arXiv preprint arXiv:2104.08500*, 2021. 2